

1 **Effect of heterogeneous aqueous reactions on the secondary**
2 **formation of inorganic aerosols during haze events**

3

4 Jiannong Quan^{1,2*}, Quan Liu^{1,2*}, Xia Li¹, Yang Gao¹, Xingcan Jia¹,
5 Jiujiang Sheng^{1,2}, Yangang Liu³

6

7

8 ¹ Beijing Key Laboratory of Cloud, Precipitation and Atmospheric Water
9 Resources, Beijing, China

10 ² Institute of Urban Meteorology, Chinese Meteorological Administration, Beijing,
11 China

12 ³Brookhaven National Laboratory, Upton, NY 11973, USA

13

14 Accepted by Atmospheric Environment
15 Sep 2015

16

17

18 **Corresponding Authors**

19

20 Jiannong Quan
21 Beijing Key Laboratory of Cloud, Precipitation and Atmospheric Water Resources,
22 Beijing, China
23 quanjn1975@gmail.com

24

25 Quan Liu
26 Beijing Key Laboratory of Cloud, Precipitation and Atmospheric Water Resources,
27 Beijing, China
28 liuquan@bjmb.gov.cn

29

30 **Abstract**

31 The effect of heterogeneous aqueous reactions on the secondary formation of inorganic
32 aerosols during haze events was investigated by analysis of comprehensive
33 measurements of aerosol composition and concentrations [e.g., particular matters
34 ($PM_{2.5}$), nitrate (NO_3), sulfate (SO_4), ammonium (NH_4)], gas-phase precursors [e.g.,
35 nitrogen oxides (NO_x), sulfur dioxide (SO_2), and ozone (O_3)], and relevant
36 meteorological parameters [e.g., visibility and relative humidity (RH)]. The
37 measurements were conducted in Beijing, China from Sep. 07, 2012 to Jan. 16, 2013.
38 The results show that the conversion ratios of N from NO_x to nitrate (N_{ratio}) and S from
39 SO_2 to sulfate (S_{ratio}) both significantly increased in haze events, suggesting enhanced
40 conversions from NO_x and SO_2 to their corresponding particle phases in the late haze
41 period. Further analysis shows that N_{ratio} and S_{ratio} increased with increasing RH,
42 with N_{ratio} and S_{ratio} being only 0.04 and 0.03, respectively, when $RH < 40\%$, and
43 increasing up to 0.16 and 0.12 when RH reached 60-80%, respectively. The enhanced
44 conversion ratios of N and S in the late haze period is likely due to heterogeneous
45 aqueous reactions, because solar radiation and thus the photochemical capacity are
46 reduced by the increases in aerosols and RH. This point was further affirmed by the
47 relationships of N_{ratio} and S_{ratio} to O_3 : the conversion ratios increase with decreasing
48 O_3 concentration when O_3 concentration is lower than <15 ppb but increased with
49 increasing O_3 when O_3 concentration is higher than 15 ppb. The results suggest that
50 heterogeneous aqueous reactions likely changed aerosols and their precursors during
51 the haze events: in the beginning of haze events, the precursor gases accumulated

52 quickly due to high emission and low reaction rate; the occurrence of heterogeneous
53 aqueous reactions in the late haze period, together with the accumulated high
54 concentrations of precursor gases such as SO₂ and NO_x, accelerated the formation of
55 secondary inorganic aerosols, and led to rapid increase of the PM_{2.5} concentration.

56

57

58 **1. Introduction**

59 Beijing has been experiencing frequent occurrence of haze events in the past two
60 decades (Che et al., 2007; Quan et al., 2011). This severe environment problem has dire
61 impacts on human health, traffic, weather and climate, and other important aspects and
62 receives growing concern in the scientific community (Charlson et al., 1987;
63 Ramanathan and Vogelmann, 1997; Tegen et al., 2000; Yu et al., 2002; Tie et al., 2009
64 a,b). In efforts to understand the mechanism of heavy haze formation and evolution in
65 Beijing, many haze-related aspects have been investigated, including aerosol
66 composition (Sun et al., 2013 a,b; 2014; Huang et al., 2014), particulate matter (PM)
67 formation mechanisms (Guo et al., 2014), regional transport of pollutants (Zhao et al.,
68 2013), hygroscopic property of particles (Pan et al., 2009; Liu et al., 2011), effects of
69 meteorology (Zhang et al., 2015), and even the feedback between aerosols and
70 meteorological variables (Quan et al., 2013; Gao et al., 2015). Large emission of
71 primary aerosols and the gaseous precursors of secondary aerosols, and stagnant
72 meteorological conditions have been usually thought as the dominant factors driving
73 the formation and evolution of haze pollution in North China Plain (NCP, Wang et al.,
74 2014; Guo et al., 2014; Zhang et al., 2015).

75 It has been reported that PM_{2.5} (particulate matter of 2.5 μm or less in aerodynamic
76 diameter) concentration could reach as high as 600 μg m⁻³ in heavy haze events (Quan
77 et al., 2014; Sun et al., 2014; Wang et al., 2014), and could increase by an order of
78 magnitude in a period of 2-4 days (Quan et al., 2014; Guo et al., 2014). Meteorological
79 conditions often play an important role in haze formation. For example, the decreased

80 height of planetary boundary layer (PBL) in haze events suppresses particles into a
81 shallower layer, and the weak wind slow down the horizontal transport. In addition to
82 the meteorology factors, secondary particle formation can make a significant
83 contribution to heavy haze events as well (Huang et al., 2014; Guo et al., 2014). Quan et
84 al. (2014) revealed that the conversion from NO_x and SO₂ to nitrate (NO₃) and sulfate
85 (SO₄) were likely accelerated in the late haze period. Because visibility and thus
86 photochemical activity are low and relative humidity (RH) increases sharply in the
87 heavy haze period, the accelerated conversion of NO_x and SO₂ might be caused by
88 heterogeneous aqueous reactions. However, up to now the effect of heterogeneous
89 aqueous reactions on secondary particle formation, especially in haze events, remains
90 poorly understood and quantified.

91 The primary objective of this work is to investigate the effect of heterogeneous aqueous
92 reactions on the secondary formation of inorganic aerosols during haze events based on
93 comprehensive measurements collected during a field campaign from Sep. 7, 2012 to
94 Jan. 16, 2013. The rest of the paper is organized as follows. Section 2 describes the
95 instruments and measurements used in this study. The results and analysis are given in
96 Section 3. The analysis focuses on (1) the variation of key variables in haze events,
97 including visibility, PM_{2.5}, NO_x, SO₂, NO₃, SO₄, and the conversion ratios of N (N_{ratio})
98 and S (S_{ratio}); (2) the relationship of N_{ratio} and S_{ratio} with RH and O₃; (3) the
99 evolution of mean particle diameter (D_{mean}) of submicron aerosols; and (4)
100 contribution of heterogeneous aqueous reactions. Section 4 provides the concluding
101 remarks.

102

103 **2. Instruments and measurements**

104 Comprehensive measurements were conducted in a field campaign at the Baolian (BL)
105 meteorological station, China Meteorological Administration (CMA) (39°56'N,
106 116°17'E). The BL station located between the west 3rd and 4th highways in Beijing.
107 The distance of the station from nearby major roads is about 400 m. The surrounding
108 region of this site is mainly residential district, without large point sources of PM_{2.5}. A
109 number of quantities, including atmospheric visibility, mass concentration of PM_{2.5},
110 chemical composition of non-refractory submicron particles (NR-PM₁), and gaseous
111 pollutants (SO₂, NO_x, CO, O₃) were measured simultaneously, together with key
112 meteorological variables of temperature, RH, pressure, wind speed, and wind direction.
113 Detailed description of above instruments was given by Quan et al. (2013; 2014).
114 Briefly, the mass concentration of PM_{2.5} was measured with a R&P model 1400a
115 Tapered Element Oscillating Microbalance (TEOM, Thermo Scientific Co., USA)
116 instrument, with a 2.5 μm cyclone inlet and an inlet humidity control system. The
117 aerosol size distribution for particles of 13 to 736 nm was obtained with a Scanning
118 Mobility Particle Sizer (SMPS, Model 3936, TSI, USA) with a time resolution of five
119 minutes. The collocated gaseous species, including CO, SO₂, NO_x and O₃, were
120 measured with various gas analyzers (Thermo Scientific Co., USA).
121 The chemical composition of NR-PM₁ was measured with an Aerodyne
122 high-resolution Time-of-Flight Aerosol Mass Spectrometer (HRToF-AMS). The
123 sampling time resolution was 5 min. The measured composition of particles included

124 sulfate (SO₄), nitrate (NO₃), ammonium (NH₄), chloride (Chl), organic aerosols (ORG).
125 The instrument was calibrated for ionization efficiency (IE) and particle sizing at the
126 beginning, middle and end of the campaign following the standard protocols (Jimenez
127 et al., 2003). The detection limits (DLs) of each NR-PM1 species were determined as 3
128 times the standard deviations (3σ) of the corresponding signals in particle-free ambient
129 air through a HEPA filter. As a result, the 5 min DLs of organics, sulfate, nitrate,
130 ammonium, and chloride were 0.058, 0.006, 0.008, 0.06 and 0.016 μg m⁻³, respectively.
131 The AMS data were analyzed for the mass concentrations and composition with the
132 standard ToF-AMS data analysis software package (SQUIRREL version 1.50 and
133 PIKA version 1.09) (Jimenez et al., 2003; DeCarlo et al., 2006). A collection efficiency
134 (CE) factor of 0.5 was introduced to account for the particle loss, mostly due to particle
135 bounce at the vaporizer (Canagaratna et al., 2007; Aiken et al., 2009; Huang et al.,
136 2010). The values of relative ionization efficiency (RIE) used in this study were 1.2 for
137 sulfate, 1.1 for nitrate, 1.3 for chloride and 1.4 for organics (Jimenez et al., 2003;
138 Canagaratna et al., 2007). The RIE value of 4.0 was used for ammonium based on the
139 analysis of pure NH₄NO₃ particles. Atmospheric visibility was measured with a
140 PWD20 (Vaisala Co., Finland), and meteorology variables were observed by WXT-510
141 (Vaisala Co., Finland).

142 **3. Results and discussion**

143 3.1. General characteristics of haze events

144 The field campaign was carried out from Sep. 07, 2012 to Jan. 16, 2013, covering
145 typical fall (Sep. 07 to Oct. 31) and winter (Nov. 01 to Jan. 16) conditions in Beijing.

146 According to the definition by CMA that a haze event satisfies when the conditions of
147 visibility ≤ 10 km and RH $< 90\%$, there were a total of 28 haze events, with an
148 averaged length of 4.7 days per haze event, during the experiment period (from Sep. 07,
149 2012 to Jan. 16, 2013). The visibility exhibits a clear periodic cycle of 4-7 days, being
150 higher than 10 km (clean) in the beginning of each cycle, and reached around 2 km
151 (polluted) within 2-4 days (Fig.1a). The measured PM_{2.5} mass concentration (Fig.1b)
152 exhibited a similar cycle, increasing from $< 50 \mu\text{g m}^{-3}$ in the beginning of haze events to
153 several hundred micrograms per cubic meter at the late stage of haze events. The NO_x
154 (Fig.1e) and SO₂ (Fig.1f), as the precursors of NO₃ and SO₄, showed a cycle similar to
155 that of PM_{2.5} concentration, with the concentrations increasing from < 10 ppb in the
156 beginning of haze events to 50-100 ppb at the late stage of haze events.

157 Previous studies indicated that the decreased atmospheric dispersion capacity in haze
158 events, characterized by lowered PBL heights and weakened wind speed (Quan et al.,
159 2013; 2014; Zhang et al., 2015), could enhance PM_{2.5} and gas pollutants concentrations.
160 Besides that, the conversion of gas phases of N and S to particle phase as measured by
161 the conversion ratios also increased in the haze events (Fig.1g). The conversion ratios
162 are defined as the ratios of the particle phase of nitrogen and sulfur to the total nitrogen
163 and sulfur (both gas and particle phases):

$$164 \quad N_{\text{ratio}} = N_a / (N_a + N_g) \quad (1)$$

$$165 \quad S_{\text{ratio}} = S_a / (S_a + S_g) \quad (2)$$

166 where (N_{ratio}) and (S_{ratio}) denote the conversion ratios of N and S, respectively; N_a is
167 the mass concentration of nitrogen in nitrate observed by HRTof-AMS; N_g is the mass

168 concentration of nitrogen in NO_x , S_a is mass concentration of sulfur in sulfate
169 observed by HRTof-AMS, and S_g is mass concentration of sulfur in SO_2 . Note that N_a
170 and S_a were measured with AMS, which only measures nitrate and sulfate in PM_{10}
171 rather than $\text{PM}_{2.5}$. The values of N_{ratio} and S_{ratio} increased from < 0.05 in the
172 beginning of haze events to 0.2 at the end of haze events. The accelerated formation of
173 secondary particles also helps to drive up $\text{PM}_{2.5}$ concentration in the haze events.

174 To get more insight into the development of haze events, the variables were classified
175 into 4 categories based on the ranges of visibility: (a) visibility > 10 km (V1) which
176 presents the non-haze days following the definition of CMA; (b) $10 \text{ km} \geq \text{visibility} > 5$
177 km (V2) for light haze days; (c) $5 \text{ km} \geq \text{visibility} > 2$ km (V3) for modest-heavy haze
178 days; and (d) $2 \text{ km} \geq \text{visibility}$ (V4) for extreme haze days. In late haze period (V4),
179 SO_2 concentration increased from 32.9 (V3) to 40.6 ppb (V4), enhanced by 23%, and
180 NO_x concentration enhanced by 18% (Table1). While for SO_4 and NO_3 , their
181 concentration enhanced by 150% and 75%, which were much higher than that of NO_x
182 and SO_2 . For $\text{PM}_{2.5}$, its concentration increased from 93.2 (V3) to $175.1 \mu\text{g m}^{-3}$ (V4),
183 enhanced by 88%. Above results indicate clearly that the conversions of gas phase of S
184 and N to particle phase were accelerated in the late haze events. To further verify this
185 point, the aerosol composition under different visibility conditions was studied. Fig.2
186 shows the percentage of different aerosol species under the different visibility
187 conditions. The mass concentrations of different aerosol species increased with the
188 development of haze events from V1 to V4. In addition, the percentages of secondary
189 aerosol particles (NO_3 , SO_4 , and NH_4) also increased. For example, in the beginning of

190 haze events (V1), the averaged aerosol concentration is low ($8.8\mu\text{g m}^{-3}$). The
191 percentage of ORG is the highest (57.3%), following by SO_4 (15.7%), NO_3 (14.6%),
192 NH_4 (9%), and Chl (3.4%). In the late period of haze events (V4), the averaged aerosol
193 concentration reached to its highest value of $97.4\mu\text{g m}^{-3}$; the percentage of ORG
194 decreased to 36.5%; the percentages of SO_4 increased to 24%; NO_3 increased to 19.4%;
195 and NH_4 increased to 15.5%. Above analysis further confirms that the secondary
196 formation of inorganic aerosols (e.g. nitrate and sulfate) was enhanced in the late period
197 of haze events.

198

199 3.2. Conversion from gas to particles phases

200 To understand the role of heterogeneous aqueous reactions in the formation of
201 secondary inorganic aerosols (e.g. NO_3 and SO_4), the relationships of N_{ratio} and S_{ratio}
202 with RH were analyzed. Fig.3 shows that N_{ratio} and S_{ratio} have no significant
203 variation when $\text{RH} < 40\%$. After $\text{RH} > 40\%$, both N_{ratio} and S_{ratio} increased with
204 further increase of RH. For example, N_{ratio} and S_{ratio} were only 0.03 and 0.03 when
205 RH was lower than 40%, and increased to 0.20 and 0.15 when RH reached 60-80%
206 (Fig.3a, Fig.3b). Some aerosol particles likely experience hygroscopic growth under
207 high RH, depending mainly on size, composition and RH. For example, the theoretical
208 deliquescence point of NaCl is about 75%, and mixing of organics could decrease the
209 deliquescence point (Hansson et al., 1998). The field experiment indicates that particles
210 begin hygroscopic growth around 40% (Pan et al., 2009). After that, the hygroscopic
211 growth factor increased exponentially. The aerosol composition in Beijing contained a

212 large amount of hydrophilic aerosol particles, such as ammonium sulfate and
213 ammonium nitrate (Sun et al., 2013a). These hydrophilic aerosol particles have a strong
214 hygroscopic property, and their radii can be doubled, or approximate 8 times increase of
215 particle volume, under high RH value (Liu et al., 2011), which provides an excellent
216 substrate for heterogeneous aqueous reactions. The increase of N_{ratio} and S_{ratio} with
217 RH (Fig.3) suggests that heterogeneous aqueous reactions play important role in the
218 secondary formation of inorganic aerosols in haze events. High photochemical activity,
219 represented by a high O_3 concentration, would further enhance the conversion ratios
220 (Fig.3).

221

222 In order to further understand the mechanisms of the formation of NO_3 and SO_4 in haze
223 events, especially the relative role of photochemical and heterogeneous aqueous
224 activities, the relationships of conversion ratios of N and S with O_3 were analyzed.
225 Fig.4 shows that N_{ratio} and S_{ratio} were the lowest when the daily-averaged O_3
226 concentration was 15-20 ppb. Above this range, the ratios increased with O_3 . For
227 example, N_{ratio} and S_{ratio} were 0.04 and 0.03 when O_3 ranging 15-20 ppb, and
228 increased to 0.23 and 0.20 when O_3 ranging 40-60 ppb. These results reflect the role of
229 photochemical activity in the formation of NO_3 and SO_4 , indicating that higher
230 photochemical capacity will enhance the conversion of gas phases of N and S to
231 particle phases. Another interesting aspect shown in Fig.4 was that the conversion
232 ratios of N and S also increased with decrease of O_3 concentration when the
233 daily-averaged O_3 concentration was lower than 15 ppb. For example, the transfer

234 ratios of N and S increased to 0.10 and 0.07 when O₃ was lower than 2 ppb. The
235 opposite changes of O₃ and RH (O₃ decreased while RH increased) reinforce the notion
236 that the increased conversion ratios of N and S was caused dominantly by
237 heterogeneous aqueous reactions.

238

239 The O₃ concentration in winter was lower than in autumn (Fig.1c), indicating that
240 photochemical capacity in winter was lower than in autumn and the relative role of
241 photochemical and heterogeneous aqueous activities in the secondary formation of
242 inorganic aerosols might be different between the two seasons. The conversion ratios of
243 N and S were higher in autumn than in winter under same RH conditions (Fig.3). For
244 example, N_{ratio} and S_{ratio} increased from 0.03 to 0.20, and 0.03 to 0.15 when RH
245 increased from <40% to 60-80% in autumn. In this process, the O₃ concentration also
246 increased from 14.6 to 26.4 ppb. While in winter, N_{ratio} and S_{ratio} only increased to
247 0.14 and 0.11, but the O₃ concentration decreased from 9.9 to 2.5 ppb. These results
248 indicate that the high conversion of S and N in haze events was caused by the combined
249 effect of photochemical and heterogeneous aqueous activity in autumn. While in winter,
250 the contribution of the heterogeneous aqueous activity became more important to the
251 formation of the secondary inorganic aerosols in haze events.

252

253 3.3. Evolution of particle size in haze events

254 To further understand the role of heterogeneous aqueous reactions in haze events,
255 evolution of particle size was analyzed. The mean particle diameter (D_{mean}) is

256 calculated as follow:

$$257 \quad D_{\text{mean}} = \sum n_i D_i / \sum n_i \quad (3)$$

258 where n_i particles are observed in the i -th bin of SMPS; D_i is the arithmetic mean
259 radius of upper and lower limitation of i -th bin. It is interesting to note that D_{mean}
260 (Fig.5b) shows a cycle similar to that of the mass concentration (Fig.5a). With the
261 development of haze events, the mean diameter increased from 50 nm to 150-200 nm in
262 2-4 days. The variation of particle number concentration (Fig.5c) was not as discernible
263 as that of particles size, indicating that the increased $\text{PM}_{2.5}$ concentration in haze events
264 was caused primarily by particle growth. As we know, atmospheric particles originate
265 from two main sources: primary emitted particles and secondary formed particles
266 arising from new particle formation (NPF) processes. After that, it grows into relevant
267 size range by condensation of chemical species such as sulfate, nitrate, and organic
268 compounds that have been partially oxidized in the atmosphere. NPF events usually
269 occur in clean condition, because high concentration of preexisting particles will
270 suppress aerosol nucleation and NPF in heavy pollution (Guo et al., 2014). Typically,
271 new particle formation and growth occur on a daily cycle in most regions worldwide
272 (Zhang et al., 2012), but few other locations exhibit particle growth as sustained (2-4 d)
273 and efficient as those displayed during the transition and polluted periods in Beijing
274 (Guo et al., 2014). In haze events, RH increased gradually (Fig.1d). Under high RH,
275 water vapor will be absorbed onto particle surface that can serve as good substrate for
276 heterogeneous aqueous reactions. Hence, the increased particle size in haze event might
277 attribute to heterogeneous aqueous reactions. We further analyze the relationship

278 between mean diameter and RH (Fig.6). The results indicate that particle size didn't
279 vary much with RH when RH <40%, but increased significantly with RH when RH >
280 40% .This result was consistent with the hygroscopic growth of aerosols under different
281 values of RH and the relationship of conversion ratios of S and N with RH discussed
282 earlier, and further lends support to the importance of heterogeneous aqueous reactions
283 in haze events.

284

285 3.4. Contributions of heterogeneous aqueous reactions in haze events

286 Secondary aerosol species contribute a major fraction of the total PM_{2.5} in Beijing
287 (Huang et al., 2014). For secondary aerosols, the variation of conversion rate in process
288 of gas to particle will affect their mass concentration directly, together with the
289 concentration of their precursor gases. Based on our measurements, the average period
290 of a haze event is 4.7 days. The averaged duration in the 4 stages were 2.02 days (V1),
291 0.90 days (V2), 1.03 days (V3), and 0.76 days (V4). In the beginning period of haze
292 events, the concentration of SO₄ increased from 1.44 μg m⁻³ (V1) to 4.67μg m⁻³ (V2),
293 with increase rate of 1.60 μg m⁻³ d⁻¹. While in the late period of haze events (V4), the
294 concentration of SO₄ increased to 23.44 μg m⁻³ (V4), with increase rate of 10.49 μg m⁻³
295 d⁻¹. The increase rate of SO₄ was significantly accelerated in the late stage (V4) of haze
296 events. While for SO₂, its concentration reached 23.5 ppb in the V2 stage, with increase
297 rate of 8.05 ppb d⁻¹, and increased to 40.5 ppb in the V4 stage, with increase rate of 9.50
298 ppb d⁻¹. The variation of NO_x and NO₃ also show similar trends. As the analysis in
299 section 3.2 and 3.3, the involvement of heterogeneous aqueous reactions might be the

300 dominant factor that accelerated the formation of SO_4 and NO_3 in the late haze events.
301 Supposing the increase rate of SO_4 in the late period were the same as the beginning
302 period, the SO_4 concentration might only reach to $7.53 \mu\text{g m}^{-3}$ in the V4 stage, much
303 lower than the actual value ($23.44 \mu\text{g m}^{-3}$). Therefore, the participation of
304 heterogeneous aqueous reactions changed the variation of aerosols and their precursors
305 in haze events. In the beginning period of haze events, the precursor gases accumulate
306 quickly due to high emission and low reaction rate. The involvement of heterogeneous
307 aqueous reactions, together with the accumulated high precursor gases, e.g. SO_2 and
308 NO_x , accelerated the formation of secondary inorganic aerosols, and led to the rapid
309 increase of $\text{PM}_{2.5}$ concentration in the late haze period.

310

311 **4. Summary**

312 The effect of heterogeneous aqueous reactions on the secondary formation of inorganic
313 aerosols in haze events are investigated by analyzing the comprehensive measurements
314 collected during a field campaign in Beijing. The major results are summarized below:

315 (1) The conversion of gas phase of S and N to particle phase was accelerated in late
316 haze events. For example, the conversion ratios, N_{ratio} and S_{ratio} , increased from
317 0.06 to 0.18, and 0.04 to 0.13 from the beginning to the late periods of haze events.

318 Analysis shows that N_{ratio} or S_{ratio} with RH increased with increasing RH when
319 RH was higher than 40%. When $\text{RH} < 40\%$, N_{ratio} or S_{ratio} showed no significant
320 variation with RH. The threshold RH of $\sim 40\%$ suggests that particles began
321 hygroscopic growth after that. Under high RH value (80%), the radius of aerosol

322 particles could be doubled by coating with the water vapor on the particle surface,
323 which provides an excellent carrier for heterogeneous aqueous reactions. This point
324 was further reinforced by the relationships of N_{ratio} and S_{ratio} with O_3
325 concentration. N_{ratio} and S_{ratio} were lowest when the daily-averaged O_3 ranges
326 between 15 and 20 ppb. Above this O_3 range, N_{ratio} and S_{ratio} increased with the
327 increase of O_3 concentration whereas N_{ratio} and S_{ratio} increased with the
328 decrease of O_3 concentration below this O_3 range. The results suggest that the
329 conversion of gas phase of S and N to particle phase might be affected by two
330 different mechanisms. Besides photochemical reactions, heterogeneous aqueous
331 reactions might also play important role in the secondary formation of inorganic
332 aerosols. The photochemical capacity usually decrease in the late period of haze
333 events due to the decreased solar radiation caused by increased aerosols, so the
334 increased conversion ratios of S and N in late haze might be caused by
335 heterogeneous aqueous reactions since RH increased evidently in this period.

336 (2) In haze events, the mean diameter of particles exhibited a cycle similar to that of the
337 $PM_{2.5}$ mass concentration. With the development of haze events, the mean diameter
338 increased from 50 nm to 150-200 nm in 2-4 days. The variation of particle number
339 concentration was not as discernible as that of particles size, indicating that the
340 increased PM mass concentration in haze events was dominated by the enhanced
341 particle size (growth). The relationship of mean diameter of particles with RH
342 indicated that the mean diameter increased with the increase of RH when RH was
343 higher than 40%, while when RH is lower than 40%, particle size did not vary much

344 with RH. The result was consistent with the relationship of N_{ratio} and S_{ratio} to RH
345 and with the hygroscopic growth of aerosols under different values of RH, and
346 further reinforced the important contribution of heterogeneous aqueous reactions in
347 haze events.

348 (3) The participation of heterogeneous aqueous reactions changed the variation of
349 aerosols and their precursors in haze events. In the beginning period of haze events,
350 the precursor gases accumulated quickly due to high emission and low reaction rate.
351 Heterogeneous aqueous reactions, together with the accumulated high precursor
352 gases (e.g. SO_2 and NO_x) accelerated the formation of secondary inorganic
353 aerosols, resulting in rapid increase of the $\text{PM}_{2.5}$ concentration in the late haze
354 period.

355 It is noteworthy that besides the conversion of SO_2/NO_x by photochemical reactions or
356 heterogeneous aqueous reactions, sulfate/nitrate might also derive from the
357 transportation from the layer above where photochemical reactivity was stronger as a
358 result of light reflection by concentrated particles below it. This process may impact
359 estimation of the role of heterogeneous aqueous reactions, and deserves in-depth study
360 in the future.

361

362 **ACKNOWLEDGMENTS:** This research is partially supported by Projects of Beijing
363 Municipal Science & Technology Commission under Grant No. Z141100001014017,
364 No.8144049. This research is also partially supported by the National Basic Research
365 Program of China (2011CB403401) and the National Natural Science Foundation of
366 China (41405127). Y. Liu is supported by the US Department of Energy's Atmospheric
367 System Research (ASR) program.

368

369 **Reference :**

370 Aiken, A.C., Salcedo, D., Cubison, M.J., Huffman, J.A., DeCarlo, P.F., Ulbrich, I.M.,
371 Docherty, K.S., Sueper, D., Kimmel, J.R., Worsnop, D.R., Trimborn, A., Northway,
372 M., Stone, E.A., Schauer, J.J., Volkamer, R.M., Fortner, E., de Foy, B., Wang, J.,
373 Laskin, A., Shutthanandan, V., Zheng, J., Zhang, R., Gaffney, J., Marley, N.A.,
374 Paredes-Miranda, G., Arnott, W.P., Molina, L.T., Sosa G., Jimenez, J.L., 2009.
375 Mexico City aerosol analysis during MILAGRO using high resolution aerosol mass
376 spectrometry at the urban supersite (T0) – Part 1: Fine particle composition and
377 organic source apportionment. *Atmos. Chem. Phys.* 9 (17), 6633-6653.

378

379 Canagaratna, M.R., Jayne, J.T., Jimenez, J.L., Allan, J.D., Alfarra, M.R., Zhang, Q.,
380 Onasch, T.B., Drewnick, F., Coe, H., Middlebrook, A., Delia, A., Williams, L.R.,
381 Trimborn, A.M., Northway, M.J., DeCarlo, P.F., Kolb, C.E., Davidovits, P.,
382 Worsnop, D.R., 2007. Chemical and microphysical characterization of ambient
383 aerosols with the aerodyne aerosol mass spectrometer. *Mass Spectrom. Rev.* 26 (2),
384 185-222.

385

386 Charlson, R.J., Lovelock, J.E., Andreae, M.O., Warren, S.G., 1987. Oceanic
387 phytoplankton, atmospheric sulfur, cloud albedo and climate. *Nature* 326, 655-661.

388

389 Che, H., Zhang, X., Li, Y., Zhou, Z., Qu, J.J., 2007. Horizontal visibility trends in China
390 1981-2005. *Geophys. Res. Lett.* 34, L24706.

391

392 DeCarlo, P.F., Kimmel, J.R., Trimborn, A., Northway, M.J., Jayne, J.T., Aiken,
393 A.C., Gonin, M., Fuhrer, K., Horvath, T., Docherty, K. S., Worsnop,
394 D. R., Jimenez, J. L., 2006. Field-Deployable, High-Resolution, Time-of-Flight
395 Aerosol Mass Spectrometer. *Anal. Chem.* 78 (24), 8281-8289.

396

397 Gao, Y., Zhang, M., Liu, Z., Wang, L., Wang, P., Xia, X., Tao, M., Zhu, L., 2015.
398 Modeling the feedback between aerosol and meteorological variables in the
399 atmospheric boundary layer during a severe fog-haze event over the North China
400 Plain. *Atmos. Chem. Phys.* 15, 4279-4295.

401

402 Guo, S., Hu, M., Zamora, M.L., Peng, J.F., Shang, D.J., Zheng, J., Du, Z., Wu, Z.,
403 Shao, M., Zeng, L., Molina, M.J., Zhang, R., 2014. Elucidating severe urban haze
404 formation in China. *Proc. Natl. Acad. Sci.* 111, 17373-17378.

405

406 Hansson, H.C., Rood, M.J., Koloutsou-Vakakis, S., Hameri, K., Orsini, D.,
407 Wiedensohler, A., 1998. NaCl Aerosol Particle Hygroscopicity Dependence on
408 Mixing with Organic Compounds. *J. Atmos. Chem.* 31, 321-346.
409

410 Huang, R.J., Zhang, Y., Bozzetti, C., Ho, K.F., Cao, J.J., Han, Y., Daellenbach, K.R.,
411 Slowik, J.G., Platt, S.M., Canonaco, F., Zotter, P., Wolf, R., Pieber, S.M., Bruns,
412 E.A., Crippa, M., Ciarelli, G., Piazzalunga, A., Schwikowski, M., Abbaszade, G.,
413 Schnelle-Kreis, J., Zimmermann, R., An, Z., Szidat, S., Baltensperger, U., El
414 Haddad, I., Prévôt, A.S., 2014. High secondary aerosol contribution to particulate
415 pollution during haze events in China. *Nature* 514, 218-222.
416

417 Huang, X.F., He, L.Y., Hu, M., Canagaratna, M.R., Sun, Y., Zhang, Q., Zhu, T., Xue, L.,
418 Zeng, L.W., Liu, X.G., Zhang, Y.H., Jayne, J.T., Ng, N.L., Worsnop, D.R., 2010.
419 Highly time-resolved chemical characterization of atmospheric submicron particles
420 during 2008 Beijing Olympic Games using an Aerodyne High-Resolution Aerosol
421 Mass Spectrometer. *Atmos. Chem. Phys.* 10, 8933-8945.
422

423 Jimenez, J.L., Jayne, J.T., Shi, Q., Kolb, C.E., Worsnop, D.R., Yourshaw, I., Seinfeld,
424 J.H., Flagan, R.C., Zhang, X., Smith, K.A., Morris, J.W., Davidovits, P., 2003.
425 Ambient aerosol sampling using the Aerodyne Aerosol Mass Spectrometer. *J.*
426 *Geophys. Res.* 108, 8425.
427

428 Liu, P.F., Zhao, C.S., Gobel, T., Hallbauer, E., Nowak, A., Ran, L., Xu, W.Y., Deng,
429 Z.Z., Ma, N., Mildenberger, K., Henning, S., Stratmann, F., Wiedensohler, A., 2011.
430 Hygroscopic properties of aerosol particles at high relative humidity and their
431 diurnal variations in the North China Plain. *Atmos. Chem. Phys.* 11, 3479-3494.
432

433 Pan, X.L., Yan, P., Tang, J., Ma, J.Z., Wang, Z.F., Gbaguidi, A., Sun, Y.L., 2009.
434 Observational study of influence of aerosol hygroscopic growth on scattering
435 coefficient over rural area near Beijing mega-city. *Atmos. Chem. Phys.* 9,
436 7519-7530.
437

438 Quan, J.N., Zhang, Q., Liu, J.Z., Huang, M.Y., Jin, H., 2011. Analysis of the formation
439 of fog and haze in North China Plain (NCP). *Atmos. Chem. Phys.* 11, 8205-8214.
440

441 Quan, J.N., Gao, Y., Zhang, Q., Tie, X.X., Cao, J., Han, S., Meng, J., Chen, P., Zhao, D.,
442 2013. Evolution of Planetary Boundary Layer under different weather conditions,
443 and its impact on aerosol concentrations. *Particuology* 11, 34-40.
444

445 Quan, J.N., Tie, X., Zhang, Q., Liu, Q., Li, X., Gao, Y., Zhao, D., 2014. Characteristics
446 of heavy aerosol pollution during the 2012-2013 winter in Beijing, China. *Atmos.*
447 *Environ.* 88, 83-89.
448

449 Ramanathan, V., Vogelmann, A.M., 1997. Greenhouse effect, atmospheric solar
450 absorption, and the Earth's radiation budget: from the Arrhenius-Lanely era to the
451 1990s. *Ambio* 26(1), 38-46.
452

453 Sun, Y.L., Wang, Z.F., Fu, P.Q., Yang, T., Jiang, Q., Dong, H.B., Li, J., Jia, J.J., 2013a.
454 Aerosol composition, sources and processes during wintertime in Beijing, China.

455 Atmos. Chem. Phys. 13, 4577-4592.
456
457 Sun, Y.L., Wang, Z., Fu, P., Jiang, Q., Yang, T., Li, J., Ge, X., 2013b. The impact of
458 relative humidity on aerosol composition and evolution processes during
459 wintertime in Beijing, China. Atmos. Environ. 77, 927-934.
460
461 Sun, Y., Jiang, Q., Wang, Z., Fu, P., Li, J., Yang, T., Yin, Y., 2014. Investigation of the
462 Sources and Evolution Processes of Severe Haze Pollution in Beijing in January
463 2013. J. Geophys. Res. 114, 4380-4398.
464
465 Tegen, I., Koch, D., Lacis, A.A., Sato, M., 2000. Trends in tropospheric aerosol loads
466 and corresponding impact on direct radiative forcing between 1950 and 1990: a
467 model study. J. Geophys. Res. 105, 26971-26990.
468
469 Tie, X., Madronich, S., Li, G.H., Ying, Z.M., Weinheimer, A., Apel, E., et al., 2009a.
470 Simulation of Mexico City Plumes during the MIRAGE-Mex Field campaign using
471 the WRF-Chem model. Atmos. Chem. Phys. 9, 4621-4638.
472
473 Tie, X., Wu, D., Brasseur, G., 2009b. Lung cancer mortality and exposure to
474 atmospheric aerosol particles in Guangzhou, China. Atmos. Environ. 43,
475 2375-2377.
476
477 Wang, Y.S., Yao, L., Wang, L.L., Liu, Z., Ji, D., Tang, G., Zhang, J., Sun, Y., Hu, B., Xin,
478 J., 2014. Mechanism for the formation of the January 2013 heavy haze pollution
479 episode over central and eastern China. Sci. China Earth Sci. 57, 14-25.
480
481 Yu, H., Liu, S.C., Dickinson, R.E., 2002. Radiative effects of aerosols on the evolution
482 of the atmospheric boundary layer. J. Geophys. Res. 107, 4142.
483 <http://dx.doi.org/10.1029/2001JD000754>.
484
485 Zhang Q., Quan, J.N., Tie, X., Li, X., Liu, Q., Gao, Y., Zhao, D., 2015. Effects of
486 meteorology and secondary particle formation on visibility during heavy haze
487 events in Beijing, China. Sci. Tot. Environ. 502, 578-584.
488
489 Zhang, R., Khalizov, A., Wang, L., Hu, M., Xu, W., 2012. Nucleation and growth of
490 nanoparticles in the atmosphere. Chem. Rev. 112(3), 1957-2011.
491
492 Zhao, P.S., Dong, F., He, D., Zhao, X.J., Zhang, X.L., Zhang, W.Z., Yao, Q., Liu, H. Y.,
493 2013. Characteristics of concentrations and chemical compositions for PM_{2.5} in
494 the region of Beijing, Tianjin, and Hebei, China. Atmos. Chem. Phys. 13,
495 4631-4644.
496
497 Zhao, X.J., Zhao, P.S., Xu, J., Meng, W., Pu, W.W., Dong, F., He, D., Shi, Q.F., 2013.
498 Analysis of a winter regional haze event and its formation mechanism in the North
499 China Plain. Atmos. Chem. Phys. 13, 5685-5696.
500

501

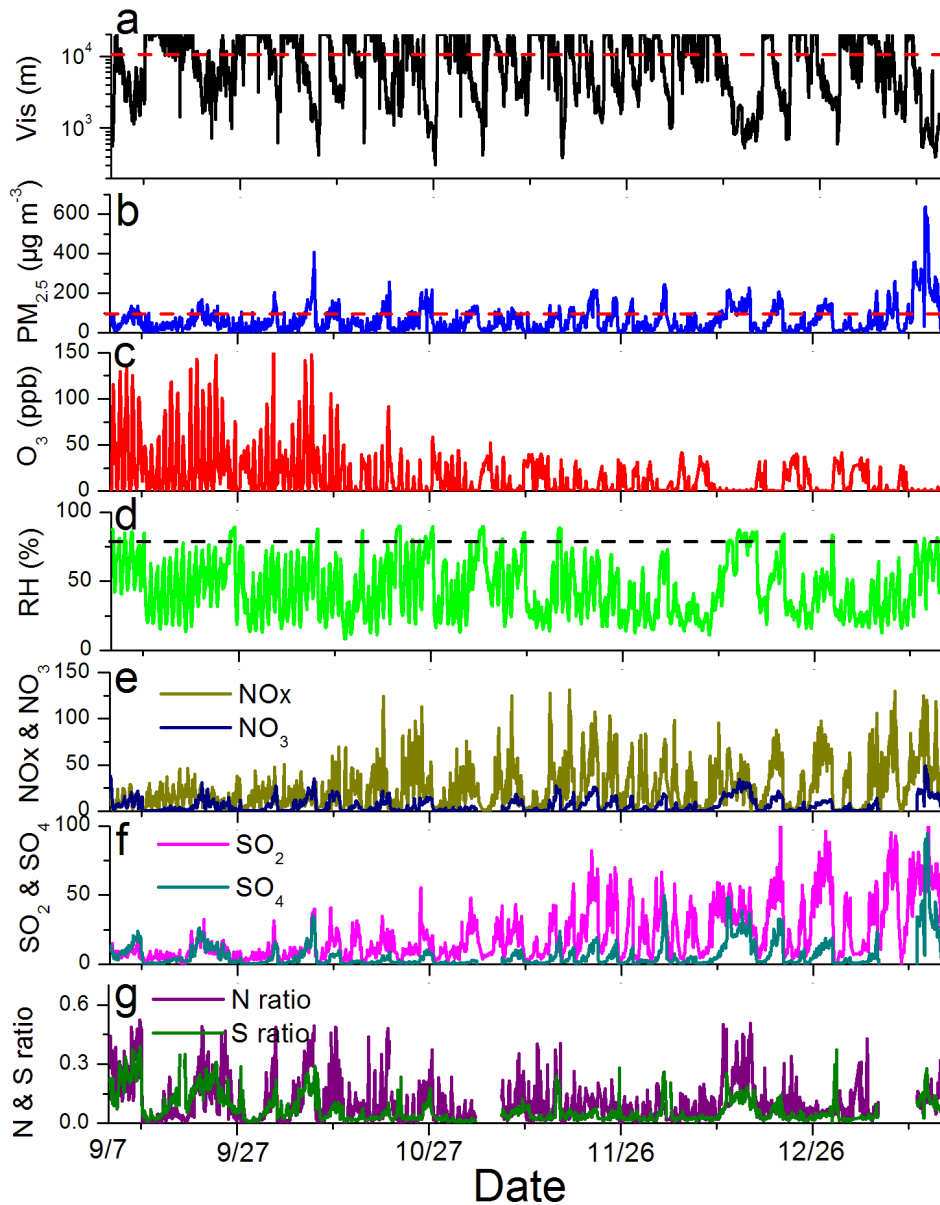
502 Table 1 Media values of measured visibility, particles, meteorological parameters,
503 chemical concentrations, and S, N ratios under different visibility ranges (V1, V2, V3,
504 and V4).

Variables	V1	V2	V3	V4
Visibility (km)	17.7	7.2	3.4	1.3
RH (%)	34.1	45.2	54.2	70.9
PM _{2.5} (µg m ⁻³)	21.7	54.0	93.2	175.1
PM ₁ (µg m ⁻³)	8.8	32.6	57.6	97.4
NO _x (ppb)	11.5	28.6	36.7	43.1
SO ₂ (ppb)	9.1	23.5	32.9	40.6
CO (ppm)	0.6	1.6	2.4	3.7
O ₃ (ppb)	19.9	14.3	15.0	4.0
N_ratio	0.06	0.10	0.15	0.18
S_ratio	0.04	0.07	0.09	0.13

505

506

507



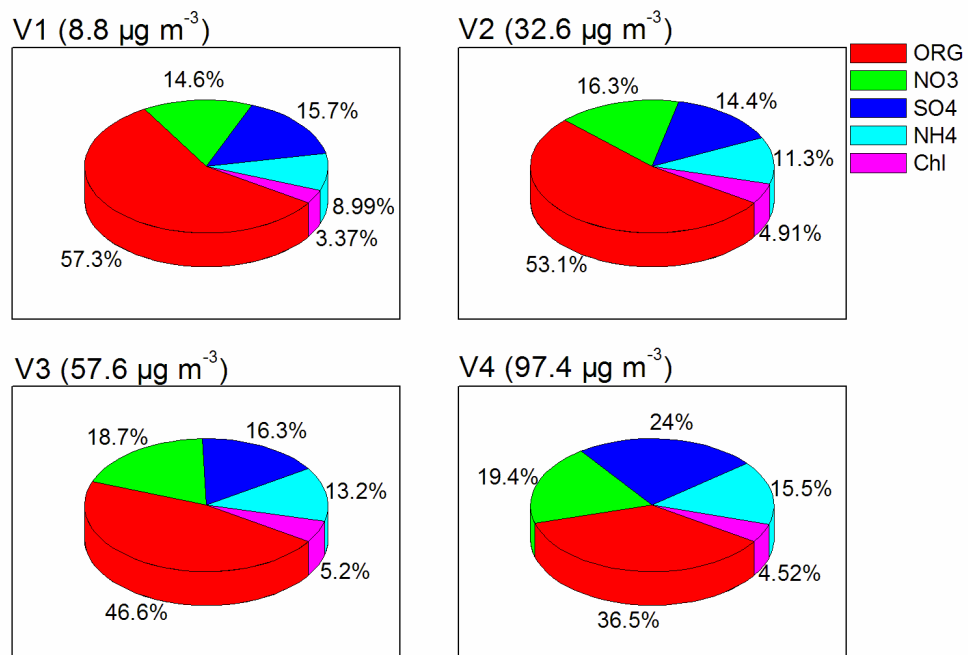
509

510

511 Fig.1 Time series of visibility (a), $PM_{2.5}$ (b), O_3 (c), RH (d), NO_x (Dark yellow, ppb)512 and NO_3 (Navy, $\mu g m^{-3}$) (e), SO_2 (Magenta, ppb) and SO_4 (Dark cyan, $\mu g m^{-3}$) (f), and N

513 (Purple) & S (Olive) conversion ratio (g), with time resolution of 1 hour.

514



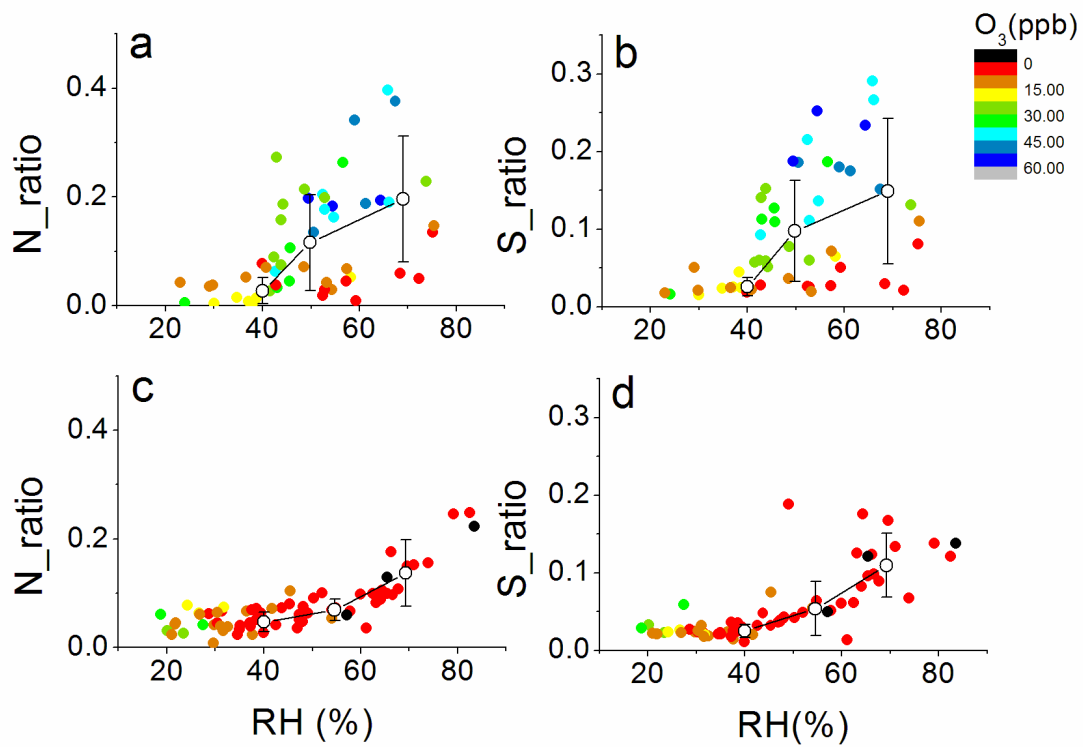
515

516 Fig.2 Aerosol composition measured by AMS under different visibility conditions. The

517 4 conditions are classified as: visibility > 10 km (V1), 10 km \geq visibility > 5 km (V2),

518 5 km \geq visibility > 2 km (V3), and 2 km \geq visibility (V4)

519



521

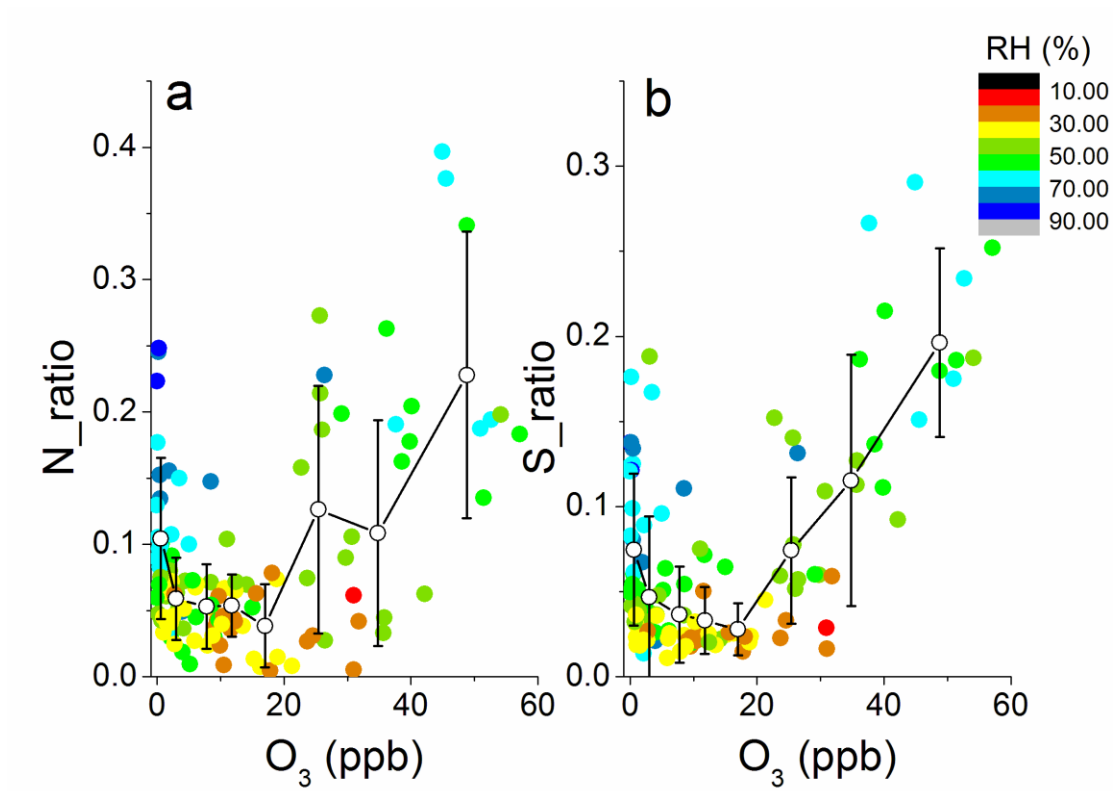
522 Fig.3 Relationship between N_ratio , S_ratio and RH in fall (a, b) and winter (c, d), with

523 time resolution of 1 day. The dot line is averaged value, with standard deviation, under

524 RH of <40%, 40-60%, 60-80%.

525

526

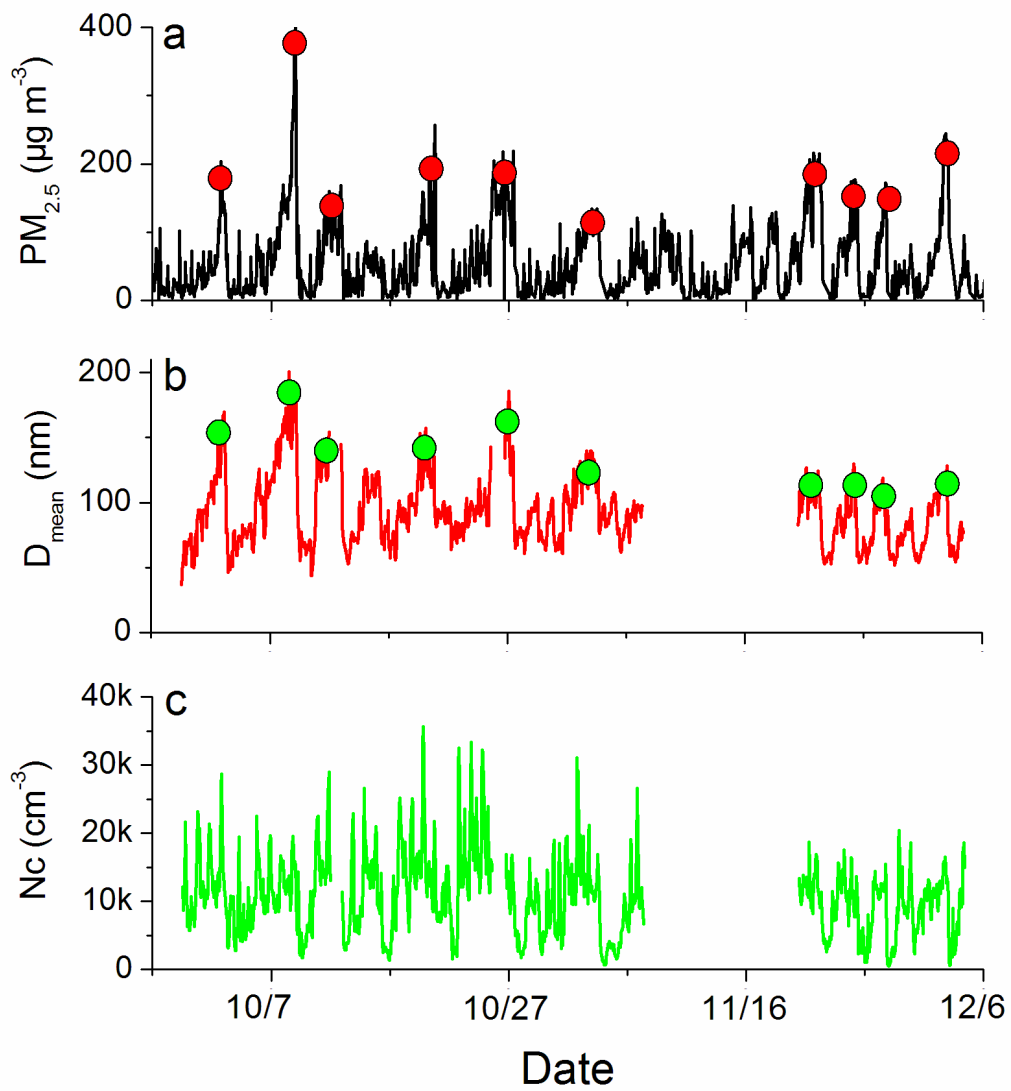


528

529 Fig.4 Relationship between N_ratio (a), S_ratio (b) and O₃, with time resolution of 1
 530 day. The dot line is averaged value, with standard deviation, under O₃ of <2, 2-5, 5-10,
 531 10-15, 15-20, 20-30, 30-40, 40-60 ppb.

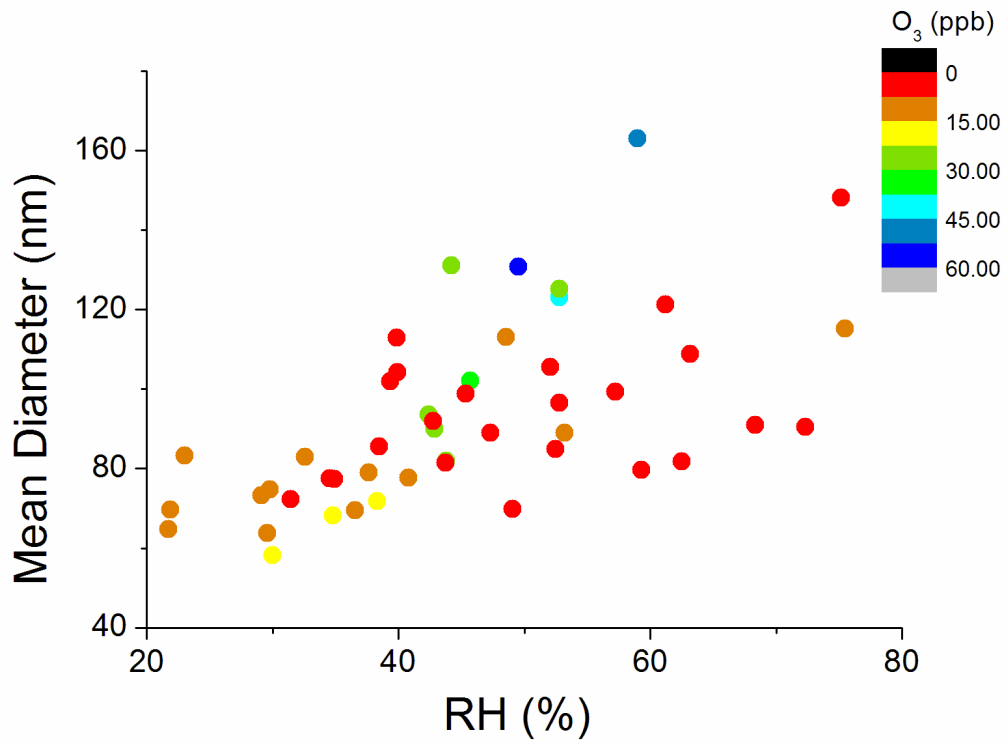
532

533
534



535
536
537
538
539

Fig.5 Time series of PM_{2.5} mass concentration(a), mean diameter (D_{mean} , b) and number concentration (N_c , c) of submicron aerosols (13-736 nm) measured by SMPS, with time resolution of 1 hour.



540

541 Fig.6 Relationship between mean diameter of submicron aerosols and RH, with time

542 resolution of 1 day.